J|A|C|S ARTICLES

Published on Web 05/21/2009

Light-Induced Oxidation of Tryptophan and Histidine. Reactivity of Aromatic *N*-Heterocycles toward Triplet-Excited Flavins

Kevin Huvaere and Leif H. Skibsted*

Food Chemistry, Department of Food Science, Faculty of Life Sciences, University of Copenhagen, Rolighedsvej 30, DK-1958 Frederiksberg C, Denmark

Received November 26, 2008; E-mail: ls@life.ku.dk

Abstract: Mechanisms of flavin-mediated photooxidation of electron-rich amino acids tryptophan and histidine were investigated for aqueous solutions. Indole, representing the tryptophan side chain in proteins, reacted at nearly diffusion controlled rates ($k \sim 2.7 \times 10^9$ L mol^{-1} s^{-1} at 293 K) with the triplet-excited flavin state, but reactions of imidazole (and histidine) were significantly slower ($k < 2.0 \times 10^8$ L mol^{-1} s^{-1}) as determined by laser flash photolysis. Oxidation rates of derivates were invariably susceptible to electronic factors affecting incipient radical cation stability, while no primary kinetic hydrogen/deuterium isotope effect was observed for imidazole. Thus reaction by electron transfer was proposed in contrast to a direct hydrogen abstraction. Unlike indole compounds, imidazole derivatives suffered from the presence of a basic imino nitrogen (=N−), which caused the rate constant of histidine free base ($k \sim 1.8 \times 10^8$ L mol^{-1} s^{-1}) to drop considerably upon protonation. Complexation of the imino nitrogen with transition metals provoked changes in reactivity, as rate constants decreased after addition of Zn^{2+} (k of 4-methylimidazole, as histidine model, decreased from 9.0×10^8 L mol^{-1} s^{-1} in the absence to 4.1×10^8 L mol^{-1} s^{-1} in the presence of $ZnCl_2$). The pyrrole nitrogen (−NH−) was not directly involved in complexation reactions, but its electron density increased upon interaction with hydrogen bond-accepting anions and resulted in higher rate constants (k of 4-methylimidazole increased from 9.0×10^8 L mol^{-1} s^{-1} to 2.0×10^9 L mol^{-1} s^{-1} after addition of NaOAc). The high rate constants were in agreement with a large thermodynamical driving force, as calculated from oxidation peak potentials determined electrochemically. After oxidation, resulting radical cations were readily deprotonated and trapped by 2-methyl-2-nitrosopropane, as detected by electron paramagnetic resonance spectroscopy. Indole-derived spin adducts were attributed to selective trapping of C(3)-centered radicals, whereas spin adducts with imidazole-derivatives arose from both carbon and nitrogen-centered imidazolyl radicals.

Introduction

Understanding the fundamentals of oxidative stress affecting proteins is an important biochemical objective, as the resulting damage to proteins has been found pivotal in the development of several pathological conditions as well as in the aging process.[1,2] Generally accepted mechanisms behind protein oxidation involve initial formation of highly reactive intermediates, including free radicals and other transient oxidants,[3,4] which target the protein backbone or sensitive side chains of constitutive amino acids.[5−7] Ensuing degradation reactions, causing loss of protein functionality and inducing protein degradation,[8,9] have been studied in model systems wherein redox partners of varying nature initiate protein oxidation.[10−12] Besides hydroxyl radicals generated by Fenton chemistry, particularly singlet oxygen ($^1O_2$, in the low-energy state denoted as $^1\Delta_g$) has attracted attention as oxidizing agent in biological systems because its specific targeting of electron-rich molecular sites, resulting in peroxide formation, was recognized as a primary cause of protein degradation.[13−15] Singlet oxygen may be formed during peroxidase activity,[13] in thermolysis of endoperoxides[16] or in a

(1) Finkel, T.; Holbrook, N. J. *Nature* **2000**, *408*, 239–247.
(2) Sohal, R. S. *Free Radical Biol. Med.* **2002**, *33*, 37–44.
(3) Halliwell, B. *J. Neurochem.* **2006**, *97*, 1634–1658.
(4) Pacher, P.; Beckman, J. S.; Liaudet, L. *Physiol. Rev.* **2007**, *87*, 315–424.
(5) Davies, K. J. A.; Delsignore, M. E.; Lin, S. W. *J. Biol. Chem.* **1987**, *262*, 9902–9907.
(6) Davies, K. J. A.; Delsignore, M. E. *J. Biol. Chem.* **1987**, *262*, 9908–9913.
(7) Rauk, A.; Armstrong, D. A. *J. Am. Chem. Soc.* **2000**, *122*, 4185–4192.
(8) Davies, K. J. A.; Lin, S. W.; Pacifici, R. E. *J. Biol. Chem.* **1987**, *262*, 9914–9920.
(9) Dean, R. T.; Thomas, S. M.; Garner, A. *Biochem. J.* **1986**, *240*, 489–494.
(10) Headlam, H. A.; Davies, M. J. *Free Radical Biol. Med.* **2004**, *36*, 1175–1184.
(11) Cooper, C. E.; Jurd, M.; Nicholls, P.; Wankasi, M. M.; Svistunenko, D. A.; Reeder, B. J.; Wilson, M. T. *Dalton Trans.* **2005**, *21*, 3483–3488.
(12) Hawkins, C. L.; Davies, M. J. *Free Radical Biol. Med.* **2005**, *39*, 900–912.
(13) Davies, M. J. *Biochem. Biophys. Res. Commun.* **2003**, *305*, 761–770.
(14) Wright, A.; Hawkins, C. L.; Davies, M. J. *Free Radical Biol. Med.* **2003**, *34*, 637–647.
(15) Agon, V. V.; Bubb, W. A.; Wright, A.; Hawkins, C. L.; Davies, M. J. *Free Radical Biol. Med.* **2006**, *40*, 698–710.
(16) Turro, N. J.; Chow, M. F.; Rigaudy, J. *J. Am. Chem. Soc.* **1981**, *103*, 7218–7224.

Haber−Weiss reaction of superoxide anion with hydrogen peroxide,[17] but the physiological occurrence of $^1O_2$ refers more often to a so-called type II photooxidation. Herein, the initial reaction step involves activation of the unreactive oxygen ground state (triplet state) through energy transfer from excited photosensitizers such as riboflavin (vitamin B_2) and its biochemical congeners, flavin mononucleotide (FMN) and flavin adenine dinucleotide (FAD). These compounds prevail in the cellular respiratory system, but also function as cofactors for specific enzymes (flavoenzymes). Human nutrition provides an essential intake, mostly through consumption of fruit and green vegetables, but substantial amounts of flavins are also found in dairy products and beverages, which, therefore, suffer from oxidative instability under light exposure.[18,19] Indeed, the presence of the isoalloxazine moiety in flavin derivates provokes significant absorption around 375 and 445 nm.[20] The high molar absorptivities (>10^4 M^{-1} cm^{-1}) involved are characteristic for $\pi-\pi^*$ transitions, which account for formation of the short-lived singlet-excited state upon irradiation.[21] Subsequent intersystem crossing generates triplet-excited flavin, which efficiently transfers excess of energy toward molecular oxygen to yield $^1O_2$. However, apart from their role as photosensitizers by definition, triplet-excited flavins are powerful oxidants ($E = +1.7$ V)[22] capable of directly interacting with various organic substrates (type I photooxidation).[23−25] Proteins were demonstrated as suitable reaction partners,[26] and, in this respect, the lethal effect of fluorescent light on human cells was ascribed to formation of cytotoxic flavin adducts with oxidized tryptophan and tyrosine residues.[27] Similar adducts have been associated with eye lens aging and the onset of cataractogenesis.[28] Since interaction most likely occurred through specific electron-rich side chains, research was focused on photooxidation of individual amino acids. The flavin-mediated light-induced degradation of cysteine and methionine was elaborated previously,[29] but detailed insights in analogous reactions of tryptophan and histidine have not been established. Therefore, a systematic approach, based on a selection of relevant tryptophan- and histidine-like substrates, was conceived to unravel fundamental reactivity of both amino acids toward triplet-excited flavins as transient oxidants. Comprehensive kinetic analyses by laser flash photolysis coupled to transient absorption spectroscopy, including the monitoring of rise and decay of short-lived flavin-derived intermediates, focused on the correlation between particular structural features and reactivity. On the other hand, thermodynamical parameters of the oxidation were derived from electron-donating properties of tryptophan and histidine derivatives, which were determined by electrochemical analyses. The study was completed by characterizing structures of incipient radical intermediates using the technique of spin trapping with subsequent electron paramagnetic resonance (EPR) spectroscopy, allowing detailed mechanisms for the photooxidation reactions to be proposed.

Experimental Section

Chemicals. L-Tryptophan and L-histidine were purchased from Merck (Darmstadt, Germany), while 1-methylpyrrole was obtained from Fluka (Buchs, Switzerland). Flavin mononucleotide and riboflavin, as well as remaining substrates for photooxidation, including deuterated compounds pyrrole-d_5 and imidazole-d_4, were supplied by Sigma-Aldrich (St. Louis, MO). Acetonitrile (Lab-Scan, Dublin, Ireland) was of spectrophotometric grade, while deuterium oxide "100" (Aldrich, St. Louis, MO) was 99.96% pure. Other chemicals used were of analytical grade. Aqueous solutions were prepared using a Milli-Q purification device (Millipore, Bedford, MA) ($R = 18.2$ MΩ cm). Buffers at 0.10 M were freshly prepared from acetic acid and sodium acetate (pH 4.0 and pH 5.0), from potassium dihydrogen phosphate and sodium hydroxide (pH 6.0, pH 7.0, and pH 8.0) or from boric acid and sodium hydroxide (pH 9.0). Buffer solutions were adjusted to constant ionic strength ($I =$ 0.16 mol L^{-1}) by addition of sodium chloride, except for buffer solutions to mix with acetonitrile.

Laser Flash Photolysis with Transient Absorption Spectroscopy. The third harmonic (355 nm, ~35 mJ $pulse^{-1}$) of a pulsed Q-switch Nd:YAG laser (Spectron Laser Systems, Rugby, U.K.) served as an excitation source for nitrogen-purged model systems, consisting of flavin mononucleotide (25 μM) and selected substrates (added in concentrations varying from 50 μM up to 20 mM). For specific experiments, reaction mixtures also included zinc(II) chloride (5.0 mM) or sodium acetate (5.0 mM). The monitoring light beam, generated by a pulsed xenon lamp (Applied Photophysics, Leatherhead, U.K.), was stripped from interfering wavelengths by installing appropriate optical filters (cutoff wavelength: ca. 610 nm and ca. 500 nm for transient absorption measurements at 720 and 520 nm, respectively). After guiding the light beam through a monochromator, transient absorption at 720 nm was measured by a 9-stage R928 photomultiplier (Hamamatsu Photonics, Hamamatsu City, Japan), whereas transient absorption at 520 nm was monitored by a 5-stage 1P28 photomultiplier (Hamamatsu Photonics). It should be noted that absorbances of triplet-excited flavin and the reduced flavin radical were competitive at 520 nm, hence, formation of the latter was monitored by subtracting the absorption trace at 720 nm, A^{720} (exclusive absorption by the triplet state), multiplied by the initial ratio A^{520}/A^{720} (for normalization), from the absorption trace at 520 nm, A^{520}.[23] Absorbances were measured under thermostatically controlled conditions at 293 K, while temperature dependence studies were carried out between 293 and 313 K.

Cyclic Voltammetry. Cyclic voltammetry experiments were carried out on a BAS CV-50W voltammetric analyzer (Bioanalytical Systems, West Lafayette, IN) using a glassy carbon electrode (BAS MF-2012) as working electrode and a platinum wire (BAS MW-1032) as auxiliary electrode. For peak potential measurements in organic solvent, substrates were dissolved in a solution of 0.10 M Bu_4NBF_4 (Aldrich, St. Louis, MO) in acetonitrile, which was purified over aluminum oxide prior to use. Potentials were referenced to a nonaqueous pseudo-reference electrode (BAS MF-2026), which was checked daily against the standard potential of the ferrocene/ferrocenium couple, Fc/Fc^+. Potentials, measured at a fixed sweep rate of 100 mV s^{-1}, were reported against the standard hydrogen electrode (SHE) by using $E° = +650$ mV vs SHE for

(17) Khan, A. U.; Kasha, M. *Proc. Nat. Acad. Sci. U.S.A.* **1994**, *91*, 12365–12367.
(18) Mortensen, G.; Bertelsen, G.; Mortensen, B. K.; Stapelfeldt, H. *Int. Dairy J.* **2004**, *14*, 85–102.
(19) Andrés-Lacueva, C.; Mattivi, F.; Tonon, D. *J. Chromatogr. A* **1998**, *823*, 355–363.
(20) Grodowski, M. S.; Veyret, B.; Weiss, K. *Photochem. Photobiol.* **1977**, *26*, 341–352.
(21) Heelis, P. F. *Chem. Soc. Rev.* **1982**, *11*, 15–39.
(22) Yoshimura, A.; Ohno, T. *Photochem. Photobiol.* **1988**, *48*, 561–565.
(23) Lu, C.-Y.; Lin, W.-Z.; Wang, W.-F.; Han, Z.-H.; Yao, S.-D.; Lin, N.-Y. *Phys. Chem. Chem. Phys.* **2000**, *2*, 329–334.
(24) Kino, K.; Saito, I.; Sugiyama, H. *J. Am. Chem. Soc.* **1998**, *120*, 7373–7374.
(25) Huvaere, K.; Olsen, K.; Andersen, M. L.; Skibsted, L. H.; Heyerick, A.; De Keukeleire, D. *Photochem. Photobiol. Sci.* **2004**, *4*, 337–340.
(26) Cardoso, D. R.; Franco, D. W.; Olsen, K.; Andersen, M. L.; Skibsted, L. H. *J. Agric. Food Chem.* **2004**, *21*, 6602–6606.
(27) Nixon, B. T.; Wang, R. J. *Photochem. Photobiol.* **1977**, *26*, 589–593.
(28) Ugarte, R.; Edwards, A.-M.; Diez, M. S.; Valenzuela, A.; Silva, E. *J. Photochem. Photobiol. B* **1992**, *13*, 161–168.
(29) Huvaere, K.; Andersen, M. L.; Storme, M.; Van Bocxlaer, J.; Skibsted, L. H.; De Keukeleire, D. *Photochem. Photobiol. Sci.* **2006**, *5*, 961–969.

the Fc/Fc^+ couple in acetonitrile.[30] A similar setup was used for peak potential determination in aqueous solution (phosphate buffer, pH 8.0, $I = 0.16$ mol L^{-1}), but the aqueous Ag/Ag^+ reference electrode (BAS MF-2052) was substituted for the nonaqueous reference electrode. In order to allow direct comparison with experiments in acetonitrile, potentials were expressed relative to SHE by including the ferrocyanide/ferricyanide couple ($E^\circ = +404$ mV vs SHE)[31] as a reference. In both experiments (aqueous and nonaqueous media), the working electrode was polished and rinsed before each measurement, while solutions were thoroughly purged with nitrogen prior to analysis. Reported peak potentials are the mean value of two independent measurements.

Electron Paramagnetic Resonance Spectroscopy. Samples for EPR analyses were prepared by dissolving substrates (10 mM) and flavin mononucleotide (25 μM) in a mixture of acetonitrile and phosphate buffer at pH 7.0 (v/v, 1:1), followed by addition of a spin trap, 5,5-dimethylpyrroline *N*-oxide (DMPO, 8−50 mM) or 2-methyl-2-nitrosopropane (MNP, 8 mM). After extensive purging with nitrogen, samples were carefully loaded into a flat quartz cell. Irradiation was carried out inside the EPR spectrometer cavity with a remote Photonics Polychrome II unit (TILL Photonics, Gräfelfing, Germany) that allowed continuous excitation of reaction mixtures at 355 nm (power ~ 0.5 mW) or at 440 nm (power ~ 2.5 mW).

EPR spectroscopy was performed on a Bruker ECS 106 spectrometer (Bruker, Karlsruhe, Germany), applying the following settings; center field, 3475 Gauss; sweep width, 80 G; microwave power, 10 mW; modulation frequency, 100 kHz; modulation amplitude, 1.0 G; conversion time, 40.96 ms; time constant, 20.48 ms. Similar settings were used to detect the indene-derived radical, which was observed in the absence of spin traps, although center field (3480 G) and modulation amplitude (down to 0.1 G) were modified. Accumulation of 4 scans resulted in the final spectrum of the spin adducts. Simulation and fitting of EPR spectra, in order to calculate hyperfine coupling constants (expressed in gauss [G]), were performed by the PEST WinSIM program.[32]

Results

Unraveling the photooxidation mechanism of tryptophan and histidine by excited flavin molecules included thorough kinetic analyses based on laser flash photolysis coupled to transient absorption spectroscopy. Since both amino acids showed no significant absorption above 300 nm, excitation by a 355 nm laser pulse was particularly suitable to generate triplet-excited flavin mononucleotide (^{3}FMN*). The ^{3}FMN* lifetime, monitored at 720 nm, fitted an exponential decay that was strongly affected by the presence of the respective substrates. Hence, bimolecular rate constants were determined from the slope of the linear dependence obtained from plotting the observed pseudo-first-order rate constants (k_{obs}) as a function of amino acid concentration. Investigation of reaction kinetics within the pH range from 4.0 to 9.0 (Figure 1) revealed that quenching of ^{3}FMN* by tryptophan approached diffusion controlled rates under neutral and acidic conditions, but reaction at high pH was slightly slower ($k_{pH7} \sim 2.6 \times 10^9$ L mol^{-1} s^{-1} vs $k_{pH9} \sim 1.7 \times 10^9$ L mol^{-1} s^{-1} at 293 K). On the other hand, quenching by histidine produced a significantly different profile, as low pH values reduced reaction efficiency due to protonation of histidine and ^{3}FMN*.[33] However, photoreaction rates increased considerably when shifting to higher pH to yield bimolecular rate constants in the order of $\sim 10^8$ L mol^{-1} s^{-1} under basic reaction conditions. The particular pH dependence of k_{obs}, which involves a set of 4 reaction paths, was accounted for by the protonation state of the two conjugated acid−base pairs, i.e. histidine ⇌ histidinium (K_{His}) and ^{3}FMN* ⇌ ^{3}[FMNH$^+$]* ($K_{Fl.1}$) (Scheme 1). Still, only 3 transition states were considered, as the composition of the histidine−^{3}[FMNH$^+$]* activated complex was indistinguishable from its histidinium−^{3}FMN* counterpart. As a result of this proton ambiguity, pH dependence of k_{obs} is determined by following entities: $k_{p,p}$, $k_{n,n}$, and the mixed middle term ($k_{p,n}K_{Fl.1} + k_{n,p}K_{His}$) (eq 1; herein, $k_{p,p}$ is the bimolecular rate constant for the reaction between the two protonated species. Likewise, $k_{n,n}$ refers to the two neutral reagents, while $k_{p,n}$ and $k_{n,p}$ are rate constants for the interactions involving one protonated species). Nonlinear curve fitting of the observed rate constants (solid line shown in Figure 1), using a $K_{Fl.1}$ value of $10^{-4.5}$,[34] eventually resulted in values of $k_{p,p} \sim 1.9 \times 10^6$ L mol^{-1} s^{-1} and $k_{n,n} \sim 1.8 \times 10^8$ L mol^{-1} s^{-1}. Tsentalovich and co-workers reported a similar pH dependence, with an equivalent value for $k_{n,n}$, but the $k_{p,p}$ term was ignored.[35] It is worth noting that the fitting process required an intriguing K_{His} shift ($10^{-7.5}$ vs the standard value of $10^{-6.1}$), a phenomenon which is normally observed for histidine residues in particular protein environments.[36] Its origin under the given circumstances remains however unclear.

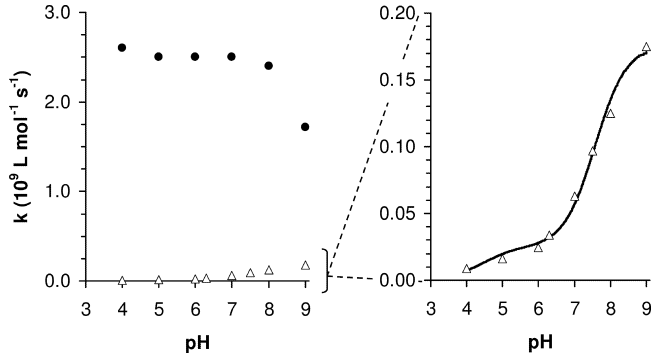

Figure 1. Left panel: The pH dependence of photooxidation rates of tryptophan (●) and histidine (Δ). Right panel: A detailed reproduction of the pH profile of histidine photooxidation rates. The solid line represents the best fit according to eq 1.

Scheme 1. The Four Bimolecular Reaction Pathways Involved in the Photooxidation of Histidine at Varying pH

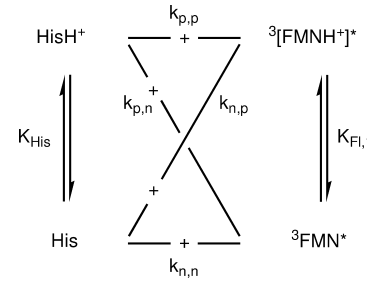

(30) Daasbjerg, K.; Pedersen, S. U.; Lund, H. In *General Aspects of the Chemistry of Radicals*; John Wiley & Sons, New York, NY, 1999; pp 385−427.
(31) McEvoy, J. P.; Foord, J. S. *Electrochim. Acta* **2005**, *50*, 2933–2941.
(32) Duling, D. R. *J. Magn. Reson., Ser. B* **1994**, *104*, 105–110.
(33) Since tryptophan oxidation was not affected by protonation of ^{3}FMN*, the pronounced effect of low pH on histidine oxidation was largely ascribed to histidinium formation.
(34) Schreiner, S.; Steiner, U.; Kramer, H. E. A. *Photochem. Photobiol.* **1975**, *21*, 81–84.
(35) Tsentalovich, Y. P.; Lopez, J. J.; Hore, P. J.; Sagdeev, R. Z. *Spectrochim. Acta A* **2002**, *58*, 2043–2050.
(36) Takahashi, T.; Nakamura, H.; Wada, A. *Biopolymers* **1992**, *32*, 897–909.

$$k_{obs} = \frac{k_{p,p}([H^+])^2 + (k_{p,n}K_{Fl,1} + k_{n,p}K_{His})([H^+]) + k_{n,n}K_{Fl,1}K_{His}}{([H^+] + K_{His})([H^+] + K_{Fl,1})} \quad (1)$$

Kinetic studies were extended by analyzing the temperature dependence of rate constants. According to transition state theory, Eyring plots, constructed from eq 2 (with h as Planck's constant and k_B as Boltzmann's constant), allowed calculation of activation parameters, including activation enthalpy ($\Delta H^{\#}$) and activation entropy ($\Delta S^{\#}$). Obviously, values of $\Delta H^{\#}$ and $\Delta S^{\#}$ obtained for histidine at neutral pH were composite values, but activation parameters determined at higher pH were practically ascribed to the reaction of histidine as free base. A comparison with the photooxidation of tryptophan, as seen in Figure 2, showed that limiting values were reached at high pH for the oxidation of both compounds.

$$\ln\left(\frac{kh}{Tk_B}\right) = \frac{\Delta S^{\#}}{R} - \frac{\Delta H^{\#}}{RT} \quad (2)$$

Photooxidation and Substrate Structure. To investigate structural features that determine reactivity toward oxidation, a comprehensive set of tryptophan and histidine derivatives was submitted to laser flash photolysis with transient absorption spectroscopy. Substrates included indole and imidazole, which are the respective side chains of the selected amino acids, as well as analogues with relevant structural variations (for structures of substrates, see Chart 1). Table 1 represents bimolecular rate constants of photoreactions, which, due to increased hydrophobic character of particular compounds, were carried out in mixed solvent (phosphate buffer at pH 7.0 with acetonitrile (v/v, 1:1)). The concurrent formation of the reduced flavin radical ($FMNH^{\bullet}$), shown in Figure 3 for interaction with 1-methylindole and 1-acetylindole, was measured at 520 nm (for details, see Experimental Section).

Since rate constants observed for imidazole varied significantly from those of indole and pyrrole, additional kinetic experiments were designed to clarify whether different reaction mechanisms were operative. Similar as for histidine, the protonation of imidazole ($pK_a \sim 6.9$)[37] affected oxidation and interaction with ^{3}FMN* resulted in a particular pH profile (Figure 4). The pH dependence of rate constants of pyrrole, which lacks the imino nitrogen, 4-methylimidazole, which serves as a histidine model due to its appropriate substitution pattern, and the *N*-protected 1,2-dimethylimidazole were also evaluated. Pyrrole behaved strikingly similarly to tryptophan, while maximum photooxidation rates of imidazole and 1,2-dimethylimidazole ($pK_a \sim 7.9$),[37] observed at pH 8, were considerably lower. On the other hand, the reaction rate of 4-methylimidazole ($pK_a \sim 7.4$)[37] amounted to $\sim 1.6 \times 10^9$ L mol^{-1} s^{-1} and closely approached that of pyrrole at pH 9. Still, the interaction of ^{3}FMN* with imidazole derivatives, including histidine, was previously associated with a hydrogen transfer, whereas an electron transfer reaction was proposed for tryptophan oxidation.[35] To discriminate between these two mechanisms, the occurrence of a primary kinetic isotope effect was searched for. Photooxidation rates of imidazole and pyrrole were determined in the absence of buffer molecules to eliminate proton exchange, while deuterium oxide was substituted for water as solvent for reactions of deuterated compounds. However, primary kinetic isotope effects (k_H/k_D), as listed in Table 2, were small and failed to support the hydrogen transfer hypothesis.

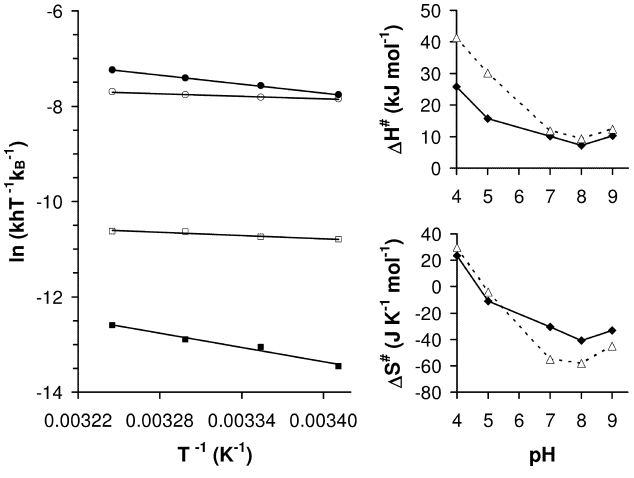

Figure 2. Left panel: Eyring plots for the photooxidation of tryptophan (at pH 4.0 (●) and at pH 8.0 (○)) and histidine (at pH 4.0 (■) and at pH 8.0 (□)), respectively. Right panel: pH dependency of activation enthalpy, $\Delta H^{\#}$ (upper graph), and activation entropy, $\Delta S^{\#}$ (lower graph), of the oxidation of tryptophan (—) and histidine (- - -), respectively.

Role of the Imino Nitrogen. Thus the discrepancy between the kinetics of tryptophan and histidine remained elusive and focus shifted toward the role of the nitrogen atoms. Imidazole and pyrrole share the presence of a pyrrole nitrogen (−NH−), which is possibly involved in hydrogen bond donation. The effect on bimolecular rate constants was readily shown by manipulating solvent accepting properties through addition of sodium acetate (NaOAc, 5.0 mM). Contrary to pyrrole (and indole), imidazole also bears a sp^2 hybridized imino nitrogen (=N−), which has been reported to serve as a ligand site for coordinating species.[38,39] Such complexation affects electronic properties as determined from measuring bimolecular rate constants in the presence of zinc chloride ($ZnCl_2$, 5.0 mM). In this respect, it should be noted that experiments were carried out in nonbuffered systems, as phosphate molecules compete for Zn^{2+} complexation. For similar purposes, riboflavin was substituted for flavin mononucleotide as light absorbing species. Bimolecular rate constants in modified reaction media, listed in Table 3, were obtained from plotting the observed pseudo-first-order rate constants (k_{obs}) as a function of the substrate concentration (as shown for 4-methylimidazole in Figure 5). The change in intercept for the reaction in the presence of Zn^{2+} probably results from interaction with flavin nitrogens. However, a control experiment with pyrrole (which lacks the imino nitrogen) showed that Zn^{2+} did not interfere with electron-accepting properties of ^{3}FMN*.

Cyclic Voltammetry. In view of determining thermodynamical feasibility of flavin-induced tryptophan and histidine photooxidation, knowledge of the reduction potentials of respective redox partners was essential. Reduction of the isoalloxazine moiety in flavin mononucleotide was expected to occur at a similar potential as reported for its riboflavin analogue, but values of tryptophan, histidine, and, particularly, their selected derivatives were determined by cyclic voltammetry. In aqueous phosphate buffer (pH 8.0, $I = 0.16$ mol L^{-1}), the lack of cathodic current

(37) Jiang, F.; McCracken, J.; Peisach, J. *J. Am. Chem. Soc.* **1990**, *112*, 9035–9044.
(38) Walker, F. A.; Lo, M.-W.; Ree, M. T. *J. Am. Chem. Soc.* **1976**, *98*, 5552–5560.
(39) Sundberg, R. J.; Martin, R. B. *Chem. Rev.* **1974**, *74*, 471–517.

Chart 1. Structures of Photooxidation Substrates (Including Derivatives of Indole, Pyrrole, and Imidazole), Flavin Compounds, and the Spin Trap 2-Methyl-2-nitrosopropane

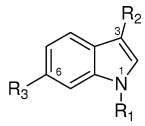

Indole: R_1=R_2=R_3=H
1-Acetylindole: R_1=C(O)CH_3; R_2=R_3=H
1-Methylindole: R_1=CH_3; R_2=R_3=H
3-Methylindole: R_1=R_3=H; R_2=CH_3
6-Methylindole: R_1=R_2=H; R_3=CH_3
Indole-3-acetic acid: R_1=R_3=H; R_2=CH_2COOH
Indole-3-propionic acid: R_1=R_3=H; R_2=CH_2CH_2COOH
Tryptamine: R_1=R_3=H; R_2=$CH_2CH_2NH_2$
Tryptophan: R_1=R_3=H; R_2=CH_2-(*S*)-CH(COOH)NH_2

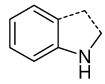

***N*-Methylaniline** (---- excl.)
Indoline (---- incl.)

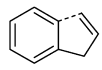

Allylbenzene (---- excl.)
Indene (---- incl.)

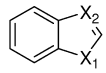

Benzofuran: X_1=O; X_2=CH
Benzimidazole: X_1=NH; X_2=N

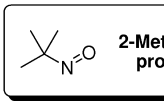

2-Methyl-2-nitroso-propane (MNP)

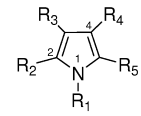

Pyrrole: R_1=R_2=R_3=R_4=R_5=H
1-Methylpyrrole: R_1=CH_3; R_2=R_3=R_4=R_5=H
1-(2-Cyanoethyl)pyrrole: R_1=$(CH_2)_2$CN; R_2=R_3=R_4=R_5=H
1,2,5-Trimethylpyrrole: R_1=R_2=R_5=CH_3; R_3=R_4=H
2,5-Dimethylpyrrole: R_1=R_3=R_4=H; R_2=R_5=CH_3
2-Boc-3,4,5-trimethylpyrrole: R_1=H; R_2=C(O)OC$(CH_3)_3$; R_3=R_4=R_5=CH_3
3-Methylpyrrole: R_1=R_2=R_4=R_5=H; R_3=CH_3
Pyrrole-2-carbaldehyde: R_1=R_3=R_4=R_5=H; R_2=C(O)H
1-Methylpyrrole-2-carbaldehyde: R_1=CH_3; R_2=C(O)H; R_3=R_4=R_5=H

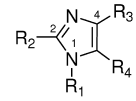

Imidazole: R_1=R_2=R_3=R_4=H
1-Methylimidazole: R_1=CH_3; R_2=R_3=R_4=H
1,2-Dimethylimidazole: R_1=R_2=CH_3; R_3=R_4=H
2-Methylimidazole: R_1=R_3=R_4=H; R_2=CH_3
2-Ethyl-4-methylimidazole: R_1=R_4=H; R_2=CH_2CH_3; R_3=CH_3
4-Methylimidazole: R_1=R_2=R_4=H; R_3=CH_3
4-Methyl-5-imidazolemethanol: R_1=R_2=H; R_3=CH_3; R_4=CH_2OH
Imidazole-4-carbaldehyde: R_1=R_2=R_4=H; R_3=C(O)H
Histamine: R_1=R_2=R_4=H; R_3=$CH_2CH_2NH_2$
Histidine: R_1=R_2=R_4=H; R_3=CH_2-(*S*)-CH(COOH)NH_2

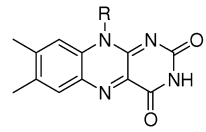

Riboflavin: R=CH_2-(*S*)-CH(OH)-(*S*)-CH(OH)-(*R*)-$CH(OH)CH_2OH$
Flavin mononucleotide: R=CH_2-(*S*)-CH(OH)-(*S*)-CH(OH)-(*R*)-CH(OH)$CH_2OP(O)(OH)O^-Na^+$

Table 1. Photooxidation Rate Constants, k (L mol^{-1} s^{-1}),[a] of Indole, Pyrrole, and Imidazole Derivates in a Mixture of Phosphate Buffer (pH 7.0) and Acetonitrile (v/v, 1:1)

compound	k	compound	k
indole derivatives		pyrrole derivatives	
tryptophan	1.8×10^9	pyrrole	3.2×10^9
1-methyltryptophan	2.7×10^9	1-methylpyrrole	2.4×10^9
tryptamine	3.9×10^9	2,5-dimethylpyrrole	3.3×10^9
indole-3-propionic acid	1.7×10^9	1,2,5-trimethylpyrrole	3.5×10^9
indole-3-acetic acid	1.7×10^9	PCA[b]	1.7×10^7
indole	2.7×10^9	imidazole derivatives	
1-methylindole	2.6×10^9	histidine	7.5×10^7
1-acetylindole	1.7×10^7	histamine	1.5×10^8
3-methylindole	2.8×10^9	imidazole	6.7×10^6
indene	5.4×10^7	1-methylimidazole	nq[c]
allylbenzene	9.6×10^5	1-acetylimidazole	nq
indoline	3.5×10^9	1,2-dimethylimidazole	1.3×10^7
aniline	2.5×10^9	2-methylimidazole	2.3×10^8
N-methylaniline	4.5×10^9	2-ethyl-4-methylimidazole	5.0×10^8
benzimidazole	9.2×10^6	4-methylimidazole	5.0×10^8
benzofuran	1.5×10^6	ICA[d]	3.0×10^5

[a] Reported values are means of duplicate analyses (experimental error ≤10%). [b] Pyrrole-2-carbaldehyde. [c] No quenching observed. [d] Imidazole-4-carbaldehyde.

in the cyclic voltammograms suggested irreversible oxidation, hence peak potentials occurred at mild overpotentials and, thus, slightly exceeded standard potential ($E°$) values. Still, the change in standard free energy for the light-induced, one-electron transfer reaction, $\Delta G°_{ET}$ (as presented in Table 4), was estimated from substituting appropriate parameters in eq 3:

$$\Delta G°_{ET} = -F(E_{ox} - E_{red}) - \Delta E_{0,0} \qquad (3)$$

Herein E_{red} is the ground state potential of the reductant (substrate) as determined from cyclic voltammetry (Table 4). The reduction potential of the oxidant (FMN/FMNH$^\bullet$ couple) is reported around −0.3 V vs NHE,[40,41] while $\Delta E_{0,0}$, the 0−0 energy gap between ground and triplet-excited state flavins,

(40) Mayhew, S. G. *Eur. J. Biochem.* **1999**, *265*, 698–702.
(41) Meisel, D.; Neta, P. *J. Phys. Chem.* **1975**, *79*, 2459–2461.

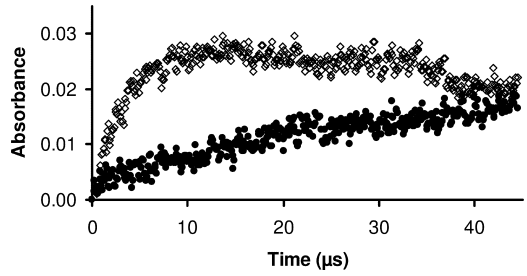

Figure 3. Formation of the reduced flavin mononucleotide radical (observed at 520 nm following laser flash photolysis at 355 nm) during photooxidation of 1-methylindole (◇) and 1-acetylindole (●).

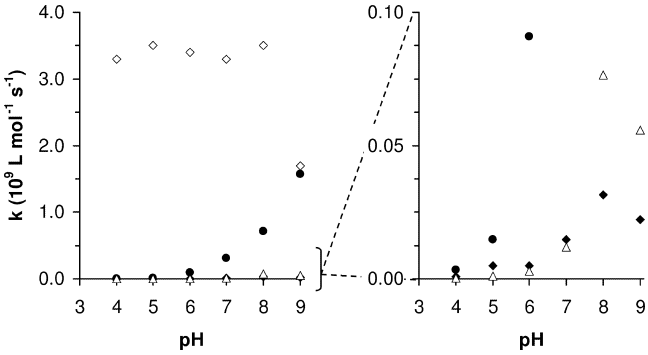

Figure 4. Left panel: The pH dependence of photooxidation rates of pyrrole (◇), imidazole (◆), 1,2-dimethylimidazole (Δ), and 4-methylimidazole (●). Right panel: A detailed reproduction of the pH profile of photooxidation rate constants with focus on imidazole and derivatives.

Table 2. Photooxidation Rate Constants, k_x (L mol^{-1} s^{-1}), of Imidazole, Pyrrole, and Their Respective Deuterated Counterparts (in Acetonitrile Mixed with Water or Deuterium Oxide)

compound	k_H[a]	compound	k_D[b]	k_H/k_D
imidazole	6.8×10^6	imidazole-d_4	4.8×10^6	1.4
pyrrole	3.2×10^9	pyrrole-d_5	2.6×10^9	1.2

[a] Rate constants determined in a mixture of acetonitrile and water (v/v, 1:1). [b] Rate constants determined in a mixture of acetonitrile and deuterium oxide (v/v, 1:1).

Table 3. Photooxidation Rate Constants, k (L mol^{-1} s^{-1}), of Selected Substrates, as Affected by the Addition of $ZnCl_2$ (5.0 mM) or NaOAc (5.0 mM)

compound	no additive	+ $ZnCl_2$	+ NaOAc
imidazole	1.4×10^7	2.3×10^6	1.9×10^7
1-methylimidazole	1.1×10^7	3.2×10^6	7.0×10^6
1,2-dimethylimidazole	1.3×10^8	2.7×10^7	1.4×10^8
2-methylimidazole	5.4×10^8	3.0×10^8	1.6×10^9
4-methylimidazole	9.0×10^8	4.1×10^8	2.0×10^9
pyrrole	3.7×10^9	3.5×10^9	4.0×10^9

amounts 210 kJ mol^{-1}.[42] Theoretically, an additional Coulombic term should be included, but its value is negligibly small in aqueous solutions and is, therefore, omitted from the equation.[43]

As a result of poor solubility of model compounds (indole derivatives in particular), several potentials were not determined in aqueous buffer. Changing to a mixed solvent, as used for laser flash photolysis, was explicitly avoided, since such conditions compromised electrochemical analyses due to severe potential drift of the reference electrode and development of

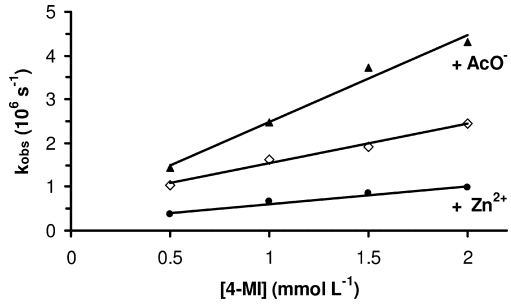

Figure 5. Plot of the observed pseudo-first-order rate constants (k_{obs}) as a function of 4-methylimidazole (4-MI) concentration (◇), affected by the presence of NaOAc (5.0 mM; ▲) and $ZnCl_2$ (5.0 mM; ●).

Table 4. Oxidation Peak Potentials, E_p (Expressed in V vs SHE), of Indole, Pyrrole and Imidazole Derivatives, as Determined in Acetonitrile (MeCN) and in Phosphate Buffer (pH 8.0), Respectively[a]

compound	E_p (MeCN)	E_p (pH 8.0)	$\Delta G°_{ET}$
indole derivatives			
tryptophan	ns[b]	0.98	−86.5
indole	1.46	ns	*c*
1-methylindole	1.39	ns	*c*
1-acetylindole	1.89	ns	*c*
3-methylindole	1.28	ns	*c*
indene	1.93	ns	*c*
benzimidazole	*d*	ns	*c*
benzofuran	2.10	ns	*c*
pyrrole derivatives			
pyrrole	1.55	1.17	−68.2
1-methylpyrrole	1.48	1.25	−60.4
PCA[e]	1.97	1.49	−37.3
MPCA[f]	1.96	1.59	−27.6
imidazole derivatives			
histidine	ns	1.50	−36.3
imidazole	1.63	1.62	−24.7
1-methylimidazole	1.92	1.72	−15.1
1,2-dimethylimidazole	1.74	1.74	−13.2
2-methylimidazole	1.65	nd[g]	*c*
4-methylimidazole	1.55	1.41	−45.0

[a] Estimated changes in standard free energy of the corresponding photooxidation, $\Delta G°_{ET}$ (in kJ mol^{-1}), are calculated from peak potentials in aqueous solutions. [b] Not soluble. [c] Peak potentials, which were determined in organic solvent, were not suitable to determine $\Delta G°_{ET}$, as flavin parameters, included in eq 3, refer to aqueous solutions. [d] Although oxidation was initiated, peak potential measurement was hampered by the anodic voltage limit of the Bu_4NBF_4/acetonitrile system. [e] Pyrrole-2-carbaldehyde. [f] 1-Methylpyrrole-2-carbaldehyde. [g] Not determined.

electrolyte deposits in electrode frits. Thus, cyclic voltammetry of indole, pyrrole, imidazole, and the respective derivatives was carried out in acetonitrile, to which 0.10 M tetrabutylammonium tetrafluoroborate (Bu_4NBF_4) was added as supporting electrolyte. In agreement with observations for tryptophan and histidine in aqueous buffer, cyclic voltammograms of these substrates showed only oxidation waves. The lack of reversibility suggested formation of highly reactive species, which readily disappeared from the reaction medium, most likely by polymerizing at the electrode surface.[44,45] The resulting insoluble film hampered heterogeneous electron transfer, which urged for thorough electrode polishing after each voltammetric cycle.

Characterization of Radical Intermediates. Since photooxidation was suggested to occur by electron abstraction, charac-

(42) Sun, M.; Moore, T. A.; Song, P.-S. *J. Am. Chem. Soc.* **1972**, *94*, 1730–1740.
(43) Rehm, D.; Weller, A. *Isr. J. Chem* **1970**, *8*, 259–271.
(44) Berlin, A.; Canavesi, A.; Schiavon, G.; Zecchin, S.; Zotti, G. *Tetrahedron* **1996**, *52*, 7947–7960.
(45) Wang, H.-L.; O'Malley, R. M.; Fernandez, J. E. *Macromolecules* **1994**, *27*, 893–901.

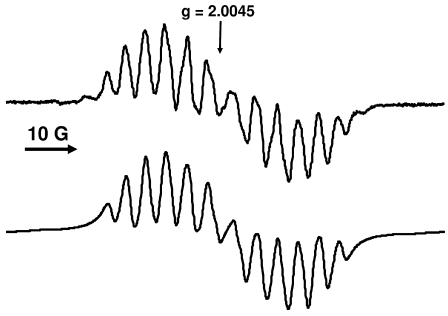

Figure 6. Experimental EPR spectrum (upper trace) recorded after photooxidation of indene by triplet-excited flavin mononucleotide (in a mixture of acetonitrile and phosphate buffer at pH 7.0 (v/v, 1:1) under nitrogen atmosphere). Coupling constants, essential for characterizing the radical structure, were obtained from the simulated spectrum (lower trace).

terization of intermediate radical species by continuous wave electron paramagnetic resonance spectroscopy (CW-EPR) was aimed at. Similar as for laser flash photolysis experiments, model systems were prepared by dissolving a particular substrate and flavin mononucleotide in a mixture of phosphate buffer (pH 7.0) and acetonitrile (v/v, 1:1). Subsequent irradiation under nitrogen atmosphere was carried out inside of the spectrometer cavity, but only indene produced a detectable radical. The intense EPR signal (Figure 6) of this species, which persisted more than 15 min after irradiation was stopped, was simulated using coupling constants 11.3 G, 9.2 G, 7.1 G, 4.6 G, 3.4 G, 3.5 G, and 3.0 G and a line width of 1.5 G.

In an attempt to obtain structural information of intermediates derived from other substrates, spin traps including 5,5-dimethyl-1-pyrroline *N*-oxide (DMPO) and 2-methyl-2-nitrosopropane (MNP) were added to the reaction mixture. Thus, highly reactive radicals were converted into spin adducts, which, due to increased stability, built up to concentrations detectable by EPR spectroscopy. Computer simulations of the resulting signals furnished essential parameters, including coupling constants and spin multiplicity, which allowed reconstruction of the incipient radical structure. DMPO, however, did not give detectable spin adducts with radicals generated by photooxidation, but distinct EPR spectra were observed with MNP as spin trapping agent. Moreover, signal intensity increased considerably when changing irradiation from 355 to 440 nm, hence the latter was preferred as excitation wavelength. Indeed, flavin absorption is stronger at 440 nm, while a higher output in lamp power was reached at longer wavelengths. With respect to these irradiation conditions, it was noted that MNP is known to be photochemically active itself,[46] but no sign of degradation was observed on exposing a spin trap solution (in acetonitrile/buffer pH 7.0) to 440 nm light. However, irradiation in the presence of FMN produced an intense triplet ($a_N \sim 16.4$ G $\pm$ 0.1) and a minor triplet of triplets ($a_N \sim 15.9$ G $\pm$ 0.1; $2 \times a_H \sim 9.5$ G $\pm$ 0.5), albeit after prolonged exposure (>30 min). Yet, addition of a substrate to the mixture of FMN and MNP provoked generation of these species shortly after irradiation was initiated. Still, their presence did not interfere with detailed analyses of substrate-derived spin patterns. A selection of experimentally obtained spectra is depicted in Figure 7, while values of coupling constants are presented in Table 5. In pursuit of unambiguous

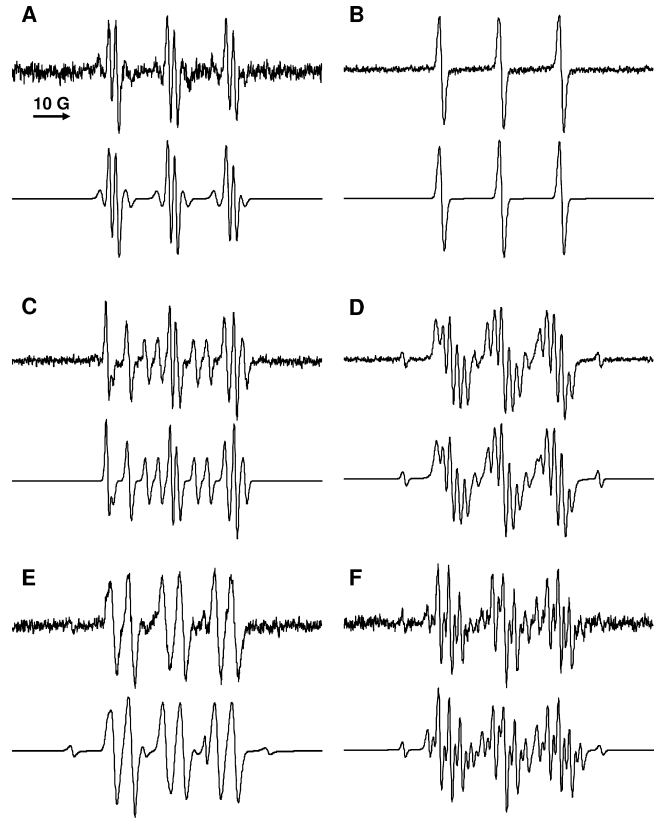

Figure 7. Experimental (upper traces) and simulated (lower traces) EPR spectra of spin adducts resulting from photooxidation of various substrates by triplet-excited flavin mononucleotide (in a mixture of acetonitrile and phosphate buffer at pH 7.0 (v/v, 1:1) under nitrogen atmosphere), followed by trapping by 2-methyl-2-nitrosopropane (MNP); (A) indole, (B) 3-methylindole, (C) pyrrole, (D) 1-methylpyrrole, (E) 2-methylimidazole, and (F) 2-ethyl-4-methylimidazole.

characterization of spin adducts, it was questioned whether one of the resolved hyperfine couplings in specific imidazole derivatives could be assigned to an exchangeable hydrogen. Therefore, irradiations were repeated in a mixture of acetonitrile and D_2O, but the spectrum of 2-ethyl-4-methylimidazole remained unaffected. On the other hand, the hydrogen coupling ($a_H \sim 3.7$ G) from the minor adduct with 4-methyl-5-imidazolemethanol collapsed in a single, unresolved line.

In addition to Table 5, it is mentioned that aniline and its derivatives, which were shown to act as very efficient electron donors toward ^{3}FMN*, failed to produce relevant spin adducts. Likewise, EPR spectra, obtained after irradiation of 1-acetylindole, benzofuran, 1-acetylimidazole, and 1-methylimidazole did not significantly differ from the spectrum observed on light exposure of a mixture containing only FMN and MNP.

Discussion

Flavin-mediated photoreactions in the absence of oxygen generally involve formation of the strongly oxidizing flavin triplet-excited state, followed by electron abstraction from various organic compounds. Tryptophan and histidine have been reported as suitable substrates,[35,47,48] but fundamental insights with respect to their reactivity have not been elaborated. Since

(46) Coyle, J. D.; Hill, R. R.; Roberts, D. R. In *Light, Chemical Change and Life: A Source Book in Photochemistry*; The Open University Press: Milton Keynes, U.K., 1982; p 57.

(47) de La Rochette, A.; Silva, E.; Birlouez-Aragon, I.; Mancini, M.; Edwards, A.-M.; Morlière, P. *Photochem. Photobiol.* **2000**, *72*, 815–820.

(48) Lu, C.-Y.; Liu, Y.-Y. *Biochim. Biophys. Acta* **2002**, *1571*, 71–76.

Table 5. Relevant Data from Simulations of the EPR Spectra of MNP Adducts with Radicals Derived from Photooxidation of Derivatives of Indole, Pyrrole, and Imidazole

compound	RA[a]	$a_{N(NO)}$[b]	$a_{N(1)}$[c]	$a_{N(3)}$[c]	a_H[d]	a_H[d]	SA[e]
indole derivates							
tryptophan	82	16.0	−	na[f]	−	−	
	18	14.0	−	na	−	−	
tryptamine	100	15.7	−	na	−	−	
indole-3-propionic acid	100	15.8	−	na	−	−	
indole-3-acetic acid	100	16.5	−	na	9.3	9.3	
indole	64	15.2	−	na	1.8	−	**iii**
	36	14.7	3.3	na	−	−	**iv**
1-methylindole	54	14.7	3.4	na	−	−	
	29	15.0	−	na	1.6	−	
	17	16.4	−	na	−	−	
3-methylindole	100	15.5	−	na	−	−	**vi**
6-methylindole	66	15.1	−	na	1.8	−	
	34	14.9	3.1	na	−	−	
pyrrole derivatives							
pyrrole	72	12.7	−	na	4.4	4.8	
	28	16.5	−	na	−	−	
1-methylpyrrole	94	13.5	1.9	na	2.1	1.4	**ix**
	4	16.0	−	na	−	−	
	2	15.9	−	na	9.6	9.0	
1-(2-cyanoethyl)pyrrole	85	13.0	1.5	na	2.8	2.0	
	8	16.0	−	na	−	−	
	7	15.9	−	na	9.6	9.1	
2-Boc-3,4,5-trimethylpyrrole[g]	94	15.5	2.2	na	−	−	**xi**
	6	15.2	−	na	−	−	
3-methylpyrrole	82	15.2	1.3	na	2.8	1.0	
	12	16.0	−	na	−	−	
	6	15.9	−	na	9.5	9.1	
imidazole derivatives							
histidine	74	13.8	1.7	−	1.1	−	
	10	16.5	−	−	−	−	
	16	15.9	−	−	9.6	9.0	
imidazole	56	10.9	2.4	1.1	2.7	−	**xiv**
	44	13.4	−	−	3.8	−	**xiii**
1,2-dimethylimidazole	66	14.1	2.5	1.6	0.9	−	
	22	14.3	−	−	11.3	11.0	
	12	16.5	−	−	−	−	
2-methylimidazole	87	13.4	−	−	4.5	−	
	8	15.9	−	−	9.6	9.1	
	5	15.9	−	−	−	−	
2-ethyl-4-methylimidazole	93	14.1	2.8	1.3	3.0	−	**xvi**
	5	16.1	−	−	−	−	
	2	16.0	−	−	9.7	9.2	
4-methylimidazole	67	14.0	2.8	1.3	2.9	−	
	31	11.6	2.2	0.7	2.9	−	
	2	15.9	−	−	9.4	9.0	
4-methyl-5-imidazolemethanol	65	14.8	2.2	2.0	1.7	−	**xx**
	35	11.8	1.2	1.6	3.7[h]	−	**xix**

[a] Relative abundance (in %). [b] Nitroxyl nitrogen (i.e., MNP nitrogen) coupling constant (in G). [c] Substrate nitrogen coupling constant (in G). [d] Substrate hydrogen coupling constant (in G). [e] Spin adduct structure (Schemes 3−5). [f] Not applicable. [g] Boc = *tert*-butoxycarbonyl. [h] Coupling disappears in D_2O.

previous investigations revealed alanine as poor substrate for flavin-induced photooxidation,[29] the highly efficient interaction between tryptophan and ^{3}FMN* was attributed to the electron-donating properties of the indole moiety. The latter lacks basic properties, hence tryptophan photooxidation was independent of reaction pH (range 4.0−8.0). At basic conditions (pH 9.0), ^{3}FMN* was deprotonated ($pK_{Fl,2} \sim 9.8$)[34] and the resulting negative charge eventually hindered electron transfer from the indole part.

Tryptophan photooxidation was enhanced by removal of the carboxylate moiety, as in tryptamine. Likewise, histamine photooxidation was faster compared to histidine, although rate constants were considerably lower than for tryptophan (and derivatives). Due to protonation of imidazole (pK_a between 6 and 7),[49] electron abstraction at acidic pH is a highly endergonic process. The high activation enthalpy ($\Delta H^{\#}$), which refers to bond breaking and bond formation in the transition state, favors hydrogen abstraction despite the lack of labile hydrogen atoms.[50] On the other hand, for reactions at higher pH the imidazole moiety prevails as free base. The associated negative activation entropy ($\Delta S^{\#}$), indicating major reorganization of the solvation shell, corroborates solvent-assisted electron transfer and formation of an ionic transition state prior to proton exchange. The pK_a of the resulting radical cation ($His^{\bullet+}$) was estimated ∼2 units higher compared to the tryptophanyl cation, $Trp^{\bullet+}$ ($pK_a \sim 4.3$),[51,52] thus solvation of the former was expected to be more pronounced. Beyond pH 8, $\Delta H^{\#}$ and $\Delta S^{\#}$ rise again, as deprotonation of ^{3}FMN* hampers electron transfer.[34]

Indole Photooxidation. The high reaction rates obtained for tryptophan and derivatives were in agreement with an electron transfer from the indole moiety to ^{3}FMN*. As such, electron-withdrawing substituents on nitrogen, as in 1-acetylindole, destabilized the intermediate radical cation and lowered the reaction rate. Concurrent formation of the reduced flavin radical anion $FMN^{\bullet-}$, which is largely protonated ($FMNH^{\bullet}$) at pH 7,[53] was considerably slower than when 1-methylindole served as substrate. Particularly the pyrrole ring accounted for electron release, since substitution of a methylene group (−CH_2−) for the pyrrole nitrogen (−NH−), as in indene, induced a 100-fold decrease of the photoreaction rate. Still, indene oxidation was assisted by the rigid carbon frame, as reaction was significantly faster than with its unrestrained analogue, allylbenzene. On the contrary, oxidation of *N*-methylaniline was faster than that of indole, probably due to removal of a π-electron from a conjugated system in the latter. The poor photooxidation rate of the isosteric benzofuran (−O− substituted for −NH−) was a result of the higher ionization potential (IP) of benzofuran (8.67 eV)[54] with respect to indole (7.76 eV),[55] as supported by a significant shift of the oxidation peak potential (Table 4). Benzimidazole (IP ∼ 8.50 eV)[56] behaved similarly.

Imidazole Photooxidation. Reaction of ^{3}FMN* with histidine is considerably slower than with tryptophan, a criterion previously used to associate the former interaction with a hydrogen transfer.[35] However, reactions of imidazole derivatives complied with properties of an electron transfer mechanism, as rates were significantly affected by the inductive effect of various substituents. The presence of a methyl group on one of the ring carbons, as in 2-methylimidazole and 4-methylimidazole, caused stabilization of the intermediate radical cation, whereas electron-withdrawing groups such as acetyl (at N(1)) and carbaldehyde (at C(4)) moieties induced opposite effects. Substrate reactivity and thermodynamical driving force of the photooxidation (listed in Table 4) were correlated, as concluded from the plot of log

(49) The $pK_a \sim 6.1$ refers to a free histidine, but this value is highly variable for histidine in protein structures. See: Edgcomb, S. P.; Murphy, K. P. *Proteins: Struct., Funct., Genet.* **2002**, *49*, 1–6.
(50) The lack of labile hydrogens was concluded from a study involving the reactivity of hydroxyl radicals with imidazole and derivatives. Herein, radical formation did not occur by hydrogen abstraction, but followed from addition of $HO^{\bullet}$ to the imidazole ring. See: Samuni, A.; Neta, P. *J. Phys. Chem.* **1973**, *77*, 1629–1635.
(51) Navaratnam, S.; Parsons, B. J. *J. Chem. Soc., Faraday Trans.* **1998**, *94*, 2577–2581.
(52) Jovanovic, S. V.; Steenken, S.; Simic, M. G. *J. Phys. Chem.* **1991**, *95*, 684–687.
(53) Heelis, P. F.; Parsons, B. J.; Phillips, G. O.; McKellar, J. F. *Photochem. Photobiol.* **1978**, *28*, 169–173.
(54) Streitwieser, A. *J. Am. Chem. Soc.* **1960**, *82*, 4123–4135.
(55) Hager, J. W.; Wallace, S. C. *Anal. Chem.* **1988**, *60*, 5–10.
(56) Palmer, M. H.; Kennedy, S. M. F. *J. Mol. Struct.* **1978**, *43*, 203–220.

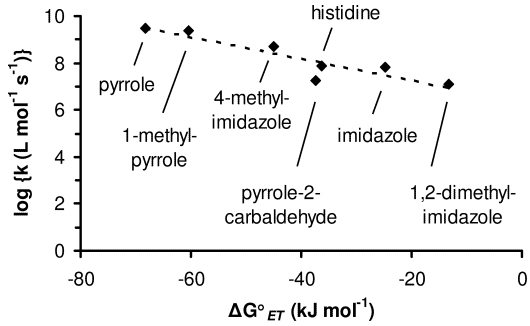

Figure 8. Plot of the log of the bimolecular rate constant (log k) vs the estimated free energy change (ΔG°_{ET}) of the photooxidation of pyrrole and imidazole derivatives.

Scheme 2. The Effect of Acetate and Zinc Ions on the Electron Density in Pyrrole and Imidazole Derivatives

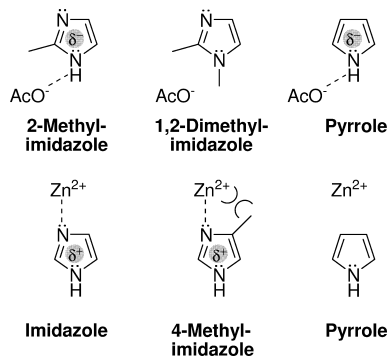

k vs standard free energy change (calculated from estimated standard potentials) of water-soluble, five-membered-ring substrates (Figure 8). The observed linear dependence is essentially considered as a linear free energy relation (LFER), since log k is proportional to the free energy of activation ($\Delta G^{\#}$). The correlation applied to pyrrole and imidazole derivates, supporting a common electron transfer mechanism. Indole compounds were not included, as no thermodynamical data was obtained from aqueous solutions.

Evidence against interaction by hydrogen transfer accumulated, as attempts to observe a primary kinetic isotope effect for imidazole photooxidation failed. Although reaction was slightly faster than with imidazole-d_4, the resulting k_H/k_D of 1.4 was too small to account for hydrogen/deuterium abstraction. Pyrrole and its deuterated counterpart, pyrrole-d_5, showed a similar behavior, but kinetic experiments unequivocally supported an electron transfer mechanism. Most likely, a change in solvent−substrate interactions was responsible for the small k_H/k_D as, for example, polarization of the N−H bond due to hydrogen bonding between pyrrole (or imidazole) and water was stronger than the corresponding N−D interaction with D_2O.[37] As a result, electron densities in pyrrole and pyrrole-d_5 differed slightly, which altered electron transfer rates. The hypothesis was confirmed when hydrogen bonding capacity of the reaction solvent was enhanced by addition of sodium acetate (NaOAc). For compounds with an unsubstituted pyrrole nitrogen (−NH−) photooxidation rates increased due to stronger polarization (Scheme 2, Table 3). The phenomenon worked synergistically with the presence of methyl substituents on the ring carbons, as unsubstituted imidazole was less sensitive than 4-methylimidazole or 2-methylimidazole. On the other hand,

Scheme 3. Irradiation of Indene, Indole, and 3-Methylindole in the Presence of Flavin Mononucleotide (FMN)[a]

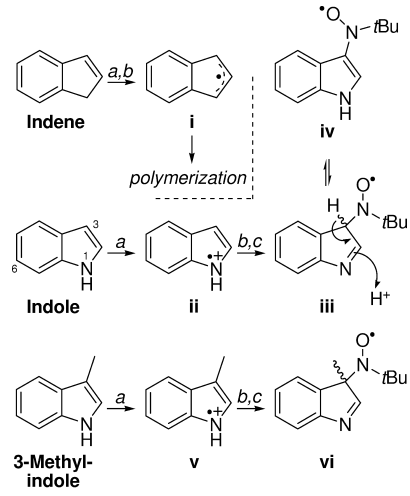

a: hν, FMN; *b*: -H+; *c*: MNP

[a] Unlike for indene, radicals derived from indole compounds were only detected after trapping by 2-methyl-2-nitrosopropane (MNP).

reaction rates of 1-methylimidazole[57] and 1,2-dimethylimidazole, which lack the ability of hydrogen bonding, remained unaffected. Also pyrrole reactivity was only slightly increased in the presence of NaOAc, as its rate constant in water (3.7×10^9 L mol^{-1} s^{-1}) already approached diffusion control.

The Distinction between Pyrrole Nitrogen and Imino Nitrogen. Hydrogen transfer failed to account for the slow imidazole photooxidation, but a pivotal role for the imino nitrogen was suspected. Its presence increased electron affinity of the entire molecule,[58] which possibly reduced electron transfer rates. Moreover, unlike the pyrrole nitrogen, the free electron pair of the imino nitrogen resides in an sp^2 hybridized orbital that extends in the plane of the five-membered ring. It is responsible for proton affinity, which led to the observed pH dependency of the imidazole photooxidation. Besides, basicity of the imino nitrogen supports a role as hydrogen bond acceptor, in contrast with hydrogen donation from the pyrrole nitrogen. The latter effect predominates in aprotic solvents as acetonitrile and explains why oxidation potentials of imidazole derivates approached those of pyrroles (Table 4). Stronger hydrogen bonding in water increased electron density in pyrrole (analogous to the example in Scheme 2) and, consequently, lowered the oxidation potential. In imidazole compounds, however, the result was opposed by hydrogen bond acceptance through the conjugated imino nitrogen. The feasibility of draining electron density via this site was illustrated from complexation with transition metal ions such as Zn^{2+}. Electron transfer to suitable redox partners was thus hampered, although 2-methylimidazole and 4-methylimidazole were less affected due to steric hindrance (Scheme 2, Table 3).[38] Pyrrole photooxidation was unaltered in the presence of zinc ions, as, obviously, the pivotal imino nitrogen was absent.

Formation of Radical Intermediates. Structural modifications affected kinetics of electron transfer significantly, but it was unclear whether such changes induced formation of different

(57) Unlike in a mixture of acetonitrile and phosphate buffer, 1-methylimidazole was readily oxidized in nonbuffered aqueous systems.
(58) Gianola, A. J.; Ichino, T.; Hoenigman, R. L.; Kato, S.; Bierbaum, V. M.; Lineberger, W. C. *J. Phys. Chem. A* **2005**, *109*, 11504–11514.

reaction intermediates. Incipient radicals, resulting from electron release (and subsequent deprotonation), were analyzed by EPR spectroscopy, but, remarkably, indene was the sole substrate to produce detectable radicals. As concluded from flash photolysis experiments with allylbenzene, oxidation of indene was favored by the release of steric constraint imposed by the sp^3 hybridized methylene. However, coupling constants in the observed spectrum failed to support formation of the initially expected planar indenyl radical (**i**, Scheme 2)[59−61] and the considerable line width pointed toward formation of polymeric species with restricted rotational motion. Indole, despite its close structural resemblance to indene, did not produce detectable EPR signals on irradiation in the presence of FMN. Indeed, indolyl radicals are highly reactive and efficient disproportionation ($2k \sim 10^8$ L mol^{-1} s^{-1}) justifies fast disappearance from the reaction medium.[52,62] Moreover, indolyl and tryptophanyl radicals possibly escaped detection as a result of recombination with flavin radicals with formation of stable adducts.[63,64] Yet, to obtain structural information of these radical intermediates, photooxidations were carried out in the presence of a spin trap. Considering the disproportionation rates of the indolyl intermediates, kinetics of DMPO trapping were most likely too slow to be efficient.[65] On the contrary, addition to MNP readily occurred and the multiplicity of the observed spin pattern correlated directly to the number of hydrogens bond to the incipient radical center. Thus, the presence of one hydrogen coupling in the spectrum of indole photooxidation (see Figure 7) suggested trapping of a secondary carbon radical (**iii**, Scheme 3). The second species was attributed to formation of a tautomeric congener of the initial adduct (**iv**). Hereby, restoration of the aromatic resonance caused loss of the hydrogen coupling, but conjugation between the nitroxyl radical and the indole nitrogen accounted for additional tripling of the signal. Direct trapping of a nitrogen-centered radical was refuted, as such mechanism was incongruous with results from 1-methylindole (*vide infra*). 6-Methylindole produced adducts identical to those from indole, hence radical addition via the C(6) position, as observed for tryptophan oxidation in lignin peroxidase,[66] was excluded. However, in contrast to indole and its 6-methyl derivative, only a single radical species was trapped after photooxidation of 3-methylindole. The methyl group at C(3) inhibited tautomeric rearrangement, but also accounted for the absence of a hydrogen coupling in the EPR spectrum. This observation supported addition of MNP at the C(3) position (**vi**), which corroborates calculated high spin density at C(3) for

Scheme 4. Photooxidation of 1-Methylpyrrole and 2-Boc-3,4,5-trimethylpyrrole and Subsequent Trapping by 2-Methyl-2-nitrosopropane (MNP)

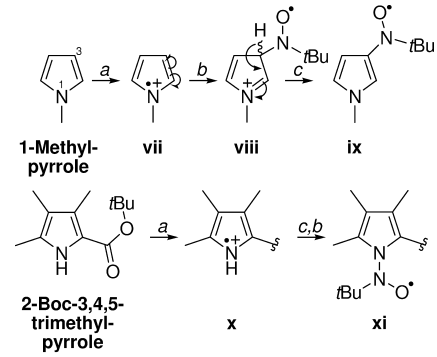

a: hv, FMN; *b*: MNP; *c*: -H^+

indolyl-type radicals (and radical cations).[67−70] Accordingly, the EPR signal from photooxidation of tryptophan was expected to resemble that of 3-methylindole,[71] but analysis was hampered by line-broadening associated with diastereomeric spin adduct formation.[72] Moreover, spin adducts observed after oxidation of $^{13}C(3)$-labeled tryptophan by dibromine radicals questioned addition via C(3).[73] Still, radicals derived from related prochiral compounds as indole-3-propionic acid (but also tryptamine) produced a 3-line spectrum that was similar to that of 3-methylindole. Only the homologous indole-3-acetic acid (a major phytohormone of the auxin class) produced a different spin adduct with coupling to two hydrogens ($2 \times a_H \sim 9.3$ G), which indicates formation of a primary carbon radical (skatole radical) as a result of decarboxylation.[74,75]

Photooxidation of 1-methylindole produced remarkably similar spectra as indole, hence formation of indole-derived adducts by direct trapping of nitrogen-centered radicals was excluded. The proposed mechanism was analogous to that of 1-methylpyrrole, although the absence of the benzene ring in combination with the extra hydrogens on the pyrrole ring changed the spectrum notably. Obviously, the *N*-methyl group prevented instant deprotonation of the incipient nitrogen-centered radical cation (rather than being involved in radical formation itself),[76] thus MNP addition initially produced an iminium-like spin adduct (**viii**, Scheme 4).[77] Subsequent stabilization pathways included release of the C(3) proton, eventually resulting in major adduct **ix**. Spin density from the nitroxyl radical was distributed in the pyrrole ring due to extensive resonance stabilization, producing the observed coupling to the pyrrole nitrogen ($a_N \sim$ 1.9 G). Coupling constants for the 3-methylpyrrole adduct were

(59) Atto, A.; Hudson, A.; Jackson, R. A.; Simmons, N. P. C. *Chem. Phys. Lett.* **1975**, *33*, 477–478.
(60) Livingston, R.; Zeldes, H.; Conradi, M. S. *J. Am. Chem. Soc.* **1979**, *101*, 4312–4319.
(61) Allen, A. D.; Tidwell, T. T. *Chem. Rev.* **2001**, *101*, 1333–1348.
(62) Candeias, L. P.; Folkes, L. K.; Dennis, M. F.; Patel, K. B.; Everett, S. A.; Stratford, M. R. L.; Wardman, P. *J. Phys. Chem.* **1994**, *98*, 10131–10137.
(63) Martin, C. B.; Tsao, M.-L.; Hadad, C. M.; Platz, M. S. *J. Am. Chem. Soc.* **2002**, *124*, 7226–7234.
(64) Silva, E.; Ugarte, R.; Andrade, A.; Edwards, A.-M. *J. Photochem. Photobiol. B* **1994**, *23*, 43–48.
(65) Taniguchi, H.; Madden, K. P. *J. Am. Chem. Soc.* **1999**, *121*, 11875–11879.
(66) Blodig, W.; Smith, A. T.; Winterhalter, K.; Piontek, K. *Arch. Biochem. Biophys.* **1999**, *370*, 86–92.
(67) Jensen, G. M.; Goodin, D. B.; Bunte, S. W. *J. Phys. Chem.* **1996**, *100*, 954–959.
(68) Walden, S. E.; Wheeler, R. A. *J. Am. Chem. Soc.* **1995**, *117*, 3175–3176.
(69) Himo, F.; Eriksson, L. A. *J. Phys. Chem. B* **1997**, *101*, 9811–9819.
(70) Huyett, J. E.; Doan, P. E.; Gurbiel, R.; Houseman, A. L. P.; Sivaraja, M.; Goodin, D. B.; Hoffman, B. M. *J. Am. Chem. Soc.* **1995**, *117*, 9033–9041.
(71) Lion, Y.; Kuwabara, M.; Riesz, P. *Photochem. Photobiol.* **1982**, *35*, 53–62.
(72) Gunther, M. R.; Kelman, D. J.; Corbett, J. T.; Mason, R. P. *J. Biol. Chem.* **1995**, *270*, 16075–16081.
(73) Candeias, L. P.; Wardman, P.; Mason, R. P. *Biophys. Chem.* **1997**, *67*, 229–237.
(74) Mottley, C.; Mason, R. P. *J. Biol. Chem.* **1986**, *261*, 16860–16864.
(75) Folkes, L. K.; Wardman, P. *Cancer Res.* **2003**, *63*, 776–779.
(76) Deprotonation and subsequent radical formation involving the *N*-methyl group was excluded due to the similarity between spin adducts arising from photooxidation of 1-(2-cyanoethyl)pyrrole and 1-methylpyrrole.
(77) The iminium-type intermediate was not directly detected during 1-methylpyrrole photooxidation, but it was associated with the MNP adduct with $a_N \sim 15.0$ G and $a_H \sim 1.6$ G when 1-methylindole served as substrate.

Scheme 5. Photooxidation of Imidazole, 2-Ethyl-4-methylimidazole, and 4-Methyl-5-imidazolemethanol and Subsequent Trapping by 2-Methyl-2-nitrosopropane (MNP)

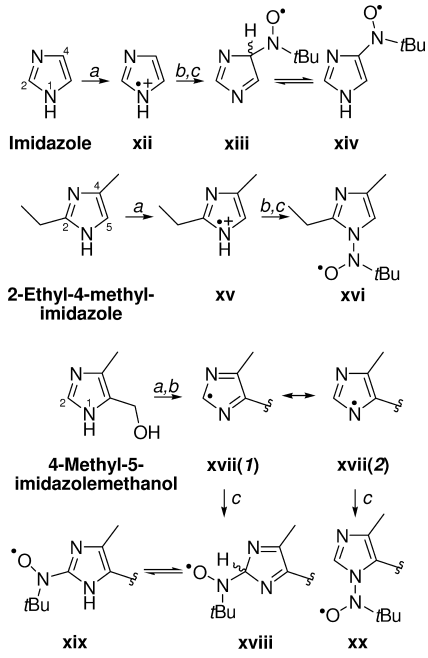

different, but unequivocal identification was difficult. However, oxidation of 2-Boc-3,4,5-trimethylpyrrole (Boc = *tert*-butoxycarbonyl), which has all carbons occupied, still showed nitrogen coupling ($a_N \sim 2.2$ G) and agreed with direct trapping of a nitrogen-centered radical (**xi**). Indeed, addition to a tertiary α-carbon radical (C(2) or C(5)) is highly unlikely due to irreversible loss of aromaticity and the introduction of considerable steric constraint. Pyrrole itself was expected to react via a similar mechanism, but observed coupling constants failed to support this. Probably fast polymerization of the incipient radical (cation) led to trapping of a derived species.

The introduction of an extra nitrogen, as in imidazole, strongly affected signals of the corresponding spin adducts. Additional hyperfine splitting was expected, but, on the other hand, the number of potential hydrogen couplings was reduced. Imidazole photooxidation involved electronic rearrangement (accompanied by proton release) of the incipient nitrogen-centered radical cation followed by addition of MNP at C(4) (**xiii**, Scheme 5). A second, major adduct showed extensive coupling, indicating aromatic properties were preserved, and formation of tautomer **xiv** was suggested. 4-Methylimidazole produced a similar (minor) species, although addition in this case was formally considered to occur at C(5). Its major adduct, however, was nearly identical to that derived from 2-ethyl-4-methylimidazole. The spectrum from the latter included coupling to a nonexchangeable proton (at C(5)), which was decisive in ascribing the adduct to direct MNP addition at the pyrrole nitrogen (**xvi**). Unfortunately, spin trapping of histidine suffered from poor spectral resolution which compromised accurate structural assignment. Still, MNP addition at C(2) after oxidation by hydrogen peroxide was previously observed,[78] but irradiation of 2-methylimidazole suggested another mechanism for photooxidation. However, obstructing access to C(4) and C(5), as in 4-methyl-5-imidazolemethanol, gave rise to 2 adducts with aromatic properties. The loss of $a_H \sim 3.7$ G in D_2O allows assignment of the minor species to MNP addition at C(2) (**xix**). Coupling constants of the second adduct remained unaffected and corroborated structure **xx**. Considering the steric influence of the amino acid moiety in histidine, a similar trapping mechanism could be expected.

Obviously, *N*-protected imidazole derivatives like 1,2-dimethylimidazole were unable to add MNP directly to the pyrrole nitrogen, but coupling to multiple nuclei still referred to extended conjugation or aromatic properties. Thus, a similar mechanism as for 1-methylindole and 1-methylpyrrole (presented in Scheme 4) was proposed, including MNP addition at C(4), which corresponds to C(3) in 1-methylpyrrole. Subsequent deprotonation reinstalls aromatic resonance and eventually furnishes an analogue of adduct **ix**. Strong hydrogen coupling in the other spin adduct assumed radical formation at one of the methyl groups as part of an alternative degradation mechanism.

Light-Induced Oxidation in Broad Perspective. The electron-rich amino acids tryptophan and histidine were found prone to photooxidation by triplet-excited flavin molecules, transient oxidants accounting for degradation of biomolecules in mammalian cells (particularly in eye and skin tissue) and in light-exposed organic matrices (e.g., food systems). The interaction was favored by a significant thermodynamical driving force, and it was concluded from a series of kinetic experiments that indole derivatives (like tryptophan) and imidazole derivatives (like histidine) were oxidized by electron abstraction from the pyrrole nitrogen. However, oxidation of histidine (and other imidazole derivatives) was strongly influenced by the presence of the imino nitrogen, as its ability to form complexes with protons, protic solvent molecules (as hydrogen bond donors), and Lewis acids caused electron density to leak. As a consequence, electron withdrawal was hindered, which is a possible mechanism for protecting histidine ligands of heme metal ions against oxidizing species (e.g., during the catalytic cycle in peroxidases). For the same reason, photooxidation via a nonradical type II mechanism (involving singlet oxygen) was considered more important than electron transfer[15,79] and histidinyl radicals were supposed to be involved only in minor degradation pathways. The interaction of singlet oxygen with tryptophan was less evident, as direct electron transfer toward triplet-excited flavins was faster than flavin-mediated formation of $^1O_2$ ($k \sim 7.0 \times 10^8$ L mol^{-1} s^{-1}) and interaction of $^1O_2$ with tryptophan ($k \sim 2.5 \times 10^8$ L mol^{-1} s^{-1}).[47] As major reaction pathway, type I photooxidation readily produced a tryptophanyl radical cation ($Trp^{\bullet+}$), a reactive intermediate that is also involved in the electron transfer reaction occurring in cytochrome *c* peroxidase.[69,70] Moreover, $Trp^{\bullet+}$ and a reduced flavin radical (derived from flavin adenine dinucleotide (FAD)) are principal species in the mechanism of DNA photolyase.[80] However, redox chemistry of the flavin chromophore in the enzyme activity is limited to the $FADH^{\bullet}/FADH^-$ couple (not $FAD/FADH^{\bullet}$), modulated by light absorption of a folate sensitizer. On the other hand, light is directly harvested by the flavin moiety in phototropins and cryptochromes (flavoproteins involved in blue-light mediated signaling pathways in plant kingdom), provoking an intramolecular electron transfer (followed by fast deprotonation) between the excited

(78) Gunther, M. R.; Peters, J. A.; Sivaneri, M. K. *J. Biol. Chem.* **2002**, *277*, 9160–9166.

(79) Luo, J.; Li, L.; Zhang, Y.; Spitz, D. R.; Buettner, G. R.; Oberley, L. W.; Domann, F. E. *Antioxid. Redox Signaling* **2006**, *8*, 1307–1314.

(80) Sancar, A. *Biochemistry* **1994**, *33*, 2–9.

flavin and tryptophan residues.[81,82] The resulting tryptophanyl radicals dissipate via back-electron transfer or interaction with neighboring tyrosine. Radicals generated by photooxidation of free tryptophan typically disappear through efficient disproportionation or addition of oxygen to form harmful peroxyl radicals. The complementary formation of flavin-derived radicals also corroborates the postulated recombination reaction with tryptophanyl radicals (preferably via the C(3) position) to produce flavin-tryptophan adducts, of which cytotoxicity and a causative role in eye-lens damage have been described.

Acknowledgment. Financial support by Arla Foods amba, the Danish Dairy Research Foundation, and the Directorate for Food, Fisheries, and Agricultural Business was gratefully accepted.

JA809039U

(81) Giovani, B.; Byrdin, M.; Ahmad, M.; Brettel, K. *Nat. Struct. Biol.* **2003**, *10*, 489–490.
(82) Zeugner, A.; Byrdin, M.; Bouly, J.-P.; Bakrim, N.; Giovani, B.; Brettel, K.; Ahmad, M. *J. Biol. Chem.* **2005**, *280*, 19437–19440.